Spatial Distribution of Cardiac Transmembrane Potentials around an Extracellular Electrode: Dependence on Fiber Orientation

Michel Neunlist*‡ and Leslie Tung‡
*INSERM U381, 67000 Strasbourg, France; and ‡Department of Biomedical Engineering, The Johns Hopkins University, Baltimore, Maryland 21205 USA

ABSTRACT Recent theoretical models of cardiac electrical stimulation or defibrillation predict a complex spatial pattern of transmembrane potential (v_m) around a stimulating electrode, resulting from the formation of virtual electrodes of reversed polarity. The pattern of membrane polarization has been attributed to the anisotropic structure of the tissue. To verify such model predictions experimentally, an optical technique using a fluorescent voltage-sensitive dye was used to map the spatial distribution of v_m around a 150-μm-radius extracellular unipolar electrode. An S1-S2 stimulation protocol was used, and v_m was measured during an S2 pulse having an intensity equal to 10× the cathodal diastolic threshold of excitation. The recordings were obtained on the endocardial surface of bullfrog atrium in directions parallel and perpendicular to the cardiac fibers. In the longitudinal fiber direction, the membrane depolarized for cathodal pulses (and hyperpolarized for anodal pulses) but only in a region within 445 ± 112 μm (and 616 ± 78 μm for anodal pulses) from the center of the electrode ($n = 9$). Outside this region, v_m reversed polarity and reached a local maximum at 922 ± 136 μm (and 988 ± 117 μm for anodal pulses) ($n = 9$). Beyond this point v_m decayed to zero over a distance of 1.5–2 mm. In the transverse fiber direction, the membrane depolarized for cathodal pulses (and hyperpolarized for anodal pulses) at all distances from the electrode. The amplitude of the response decreased with distance from the electrode with an exponential decay constant of 343 ± 110 μm for cathodal pulses and 253 ± 91 μm for anodal pulses ($n = 7$). The results were qualitatively similar in both fiber directions when the atrium was bathed in a solution containing ionic channel blockers. A two-dimensional computer model was formulated for the case of highly anisotropic cardiac tissue and qualitatively accounts for nearly all the observed spatial and temporal behavior of v_m in the two fiber directions. The relationships between v_m and both the "activating function" and extracellular potential gradient are discussed.

INTRODUCTION

The anisotropic structure of the heart has been shown to influence various electrical events occurring in the normal and pathologic heart. It accounts for directional differences in conduction velocity (Roberts et al., 1979), action potential duration (Osaka et al., 1987), excitation thresholds (Frazier et al., 1988), and prolongation of repolarization by electrical stimulation (Knisley et al., 1993). Under pathological conditions, such as in an infarcted region of the myocardium, the anisotropic structure is an important factor in the initiation and maintenance of sustained arrhythmias (Dillon et al., 1988; Lesh et al., 1991). In addition, recent experimental studies have demonstrated the importance of fiber orientation in the electrical initiation of reentry or fibrillation (Knisley et al., 1992; Chen et al., 1993). Computer models of the heart now take into account the anisotropy of myocardial electrical conductivities (Sepulveda et al., 1989; Roth, 1992; Saypol and Roth, 1993).

One example that has been relatively well characterized theoretically is the influence of fiber orientation on the pattern of transmembrane potentials (V_m) around an extracellular stimulating electrode during the stimulus pulse. The anisotropic bidomain model represents the intracellular and extracellular spaces of cardiac muscle as continuous conductive domains that coexist at each point in space and are coupled through the cell membrane (Henriquez, 1993). Each domain can be electrically anisotropic and characterized by a conductivity tensor. Under physiological conditions, the cardiac fibers are approximately parallel, with a ratio of longitudinal to transverse conductivities that is greater in the intracellular domain than in the extracellular domain. In this case, the bidomain model predicts a primary region of depolarization for cathodal pulses (and hyperpolarization for anodal pulses) having a "dog-bone" shape in a direction perpendicular to the fiber direction and secondary, oppositely polarized regions along the fiber direction (Sepulveda et al., 1989; Roth, 1992). The formulation of oppositely polarized

Received for publication 3 June 1994 and in final form 30 December 1994.

Address reprint requests to Dr. Leslie Tung, Department of Biomedical Engineering, Johns Hopkins University, 720 Rutland Avenue, Baltimore, MD 21205. Tel.: 410-955-7453; FAX: 410-955-0549; E-mail: ltung@bme.jhu.ed.

Abbreviations used: ARP, absolute refractory period of the action potential; CDT, cathodal diastolic threshold for excitation; C_m, specific membrane capacitance (units of μF/cm²); F, baseline fluorescence level from voltage-sensitive dye; ΔF, change in fluorescence associated with V_m; r_e, extracellular longitudinal resistance of cardiac fiber (units of Ω/cm); r_i, intracellular longitudinal resistance of cardiac fiber (units of Ω/cm); R_m, specific membrane resistance (units of kΩ-cm²); S, activating function; S1, stimulus pulse applied during rest; S2, second stimulus pulse applied after an S1 pulse, with a delay referred to as the S1–S2 interval; V_e, extracellular (interstitial) potential; $\nabla_x V_e$, extracellular potential gradient in the x direction; V_m, cellular transmembrane potential; v_m, the change in V_m resulting from an electrical stimulus pulse, relative to V_m in the absence of the pulse; W, step response of fiber to an extracellular point source of current; λ, tissue or fiber space constant; τ, monoexponential time constant that describes the initial temporal response of v_m to a step in stimulus current; τ_m, membrane time constant; σ_{ix}, σ_{iy}, conductivities of the intracellular domain along the x and y directions, respectively; σ_{ex}, σ_{ey}, conductivities of the extracellular domain along the x and y directions, respectively.

0006-3495/95/06/2310/13 $2.00

virtual electrodes may be significant in explaining anodal stimulation (Roth, 1992; Neunlist and Tung, 1994a; Knisley et al., 1994). The dog-bone shape of the primary electrode has been inferred experimentally by Wikswo et al. (1991) in the canine ventricle by measuring the time for electrical activity to propagate from the stimulus electrode to various recording sites. However, their experiments did not directly measure V_m during the stimulus pulse and therefore could be influenced by factors such as variable latency time for activation (Krassowska et al., 1992).

Direct measurements of the V_m response during a stimulating pulse, although they are desirable, are faced with technical difficulties. With conventional (microelectrode) recording techniques it is difficult to record the induced changes in V_m free of electrical artifact in the vicinity of the stimulating electrode, especially at high current densities. To circumvent this problem, one can exploit the property that voltage-sensitive dyes are insensitive to potential gradients in the tissue and can measure true changes in V_m (Salama, 1988). Although this property was first observed in heart preparations nearly 20 years ago (Salama and Morad, 1976), voltage-sensitive dyes have been used in cardiac research primarily to map the spread of excitation (Salama, 1988) and to characterize changes in action potential duration (Dillon, 1992). Recently, the dyes have been used to document the changes in V_m during the pulse itself (Dillon and Wit, 1988; Tung et al., 1991; Neunlist et al., 1992; Windisch et al., 1992; Knisley et al., 1994; Neunlist and Tung, 1994a; Tung et al., 1994).

The goal of this paper is to test the predictions of the anisotropic bidomain model of the V_m responses in the longitudinal and transverse fiber directions. We present an experimental and modeling study of the spatial and temporal changes in transmembrane potential V_m near an extracellular electrode in the bullfrog atrium. Preliminary results have been presented in abstract form (Neunlist and Tung, 1994b).

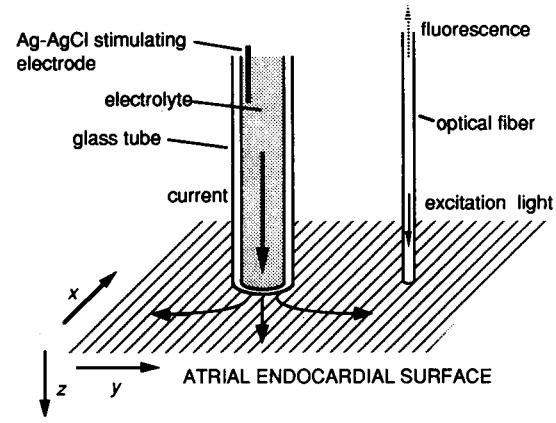

FIGURE 1 Optical measurement of transmembrane potentials. An optical fiber ("optrode") was used to carry excitatory light to and fluorescent light from the experimental preparation stained with the voltage-sensitive dye di-4-ANEPPS. The fiber was attached to the tip of a supporting glass pipette, mounted to a micromanipulator (not shown). The "optrode" was used to record electro-optical transmembrane signals at different surface sites around the stimulating pipette.

MATERIALS AND METHODS

Optical recording system

The optical setup was slightly modified from that described in a previous paper (Neunlist et al., 1992). Briefly, it consisted of a portable fluorimeter coupled to an optical fiber. The optical fiber carried both the excitation light from the laser and the fluorescence emitted by the preparation stained with voltage-sensitive dye. The fluorescence was measured by a custom-built photodiode system. The signal was digitized through a data-acquisition card (LabVIEW, National Instruments, Austin, TX) in a personal computer (Macintosh IIx, Apple Computer, Cupertino, CA). The overall bandwidth of the measured optical signal was 0–3 kHz. The fiber tip could be positioned with a micromanipulator in the tissue region adjacent to the stimulating electrode (Fig. 1). Its position relative to the edge of the stimulating electrode was measured with an eyepiece micrometer having approximately 12.5-μm resolution.

Preparation

All experiments were performed at room temperature (20–25°C) on the atria of bullfrog (*Rana catesbeiana*) hearts. The frogs were decapitated and double pithed. The heart was rapidly removed and washed out with Ca-containing Ringer solution. The atria were then carefully dissected and removed from the ventricle and then cut open. The septum was removed and the remaining tissue pinned down in a Sylgard-coated dish with the endocardial surface facing upward. The sinus venosus and the atrioventricular cells were removed to prevent pacing automaticity. The endocardial surface consists of numerous bundles 100–300 μm in diameter, running in approximately the same direction over a length scale of several millimeters (Fig. 2 *A*). The tissue was incubated in the dark for 10 min with 30 μM of the voltage-sensitive dye di-4-ANEPPS (in 0.3% dimethyl sulfoxide) in a 0.5-mM Ca Ringer solution. Afterward the tissue was washed out with a dye-free Ca Ringer solution.

We chose the bullfrog atrium for this study for two reasons: first, it has distinct, large (100–300-μm diameter) fiber bundles, allowing us a clear identification of the fiber direction. Second, its size once it is pinned open (approximately 1 × 1.5 cm) is large enough and thin enough that boundary effects from the edge of the preparation can be neglected when one is recording in the central region of the atrium.

Stimulus electrode

The preparation was stimulated by a constant-current monophasic square pulse. The pulses were delivered through a glass pipette filled with Ringer solution from the bath and connected to a Grass stimulator by a Ag–AgCl wire. The stimulating pipette was mounted in a modified microelectrode holder attached to a micromanipulator. The tip of the stimulating pipette had an internal radius of 150 μm and was positioned approximately 100–200 μm above the atrial surface. The amplitude of the stimulus current was monitored by the voltage drop across a resistor in series with the electrodes. The return electrode consisted of a pair of Pt wires positioned 2 cm away on either side of the tissue.

Stimulation protocol

To study better the tissue response as related to its fiber structure and not to activation of Na currents, we applied test pulses during the ARP of the action potential. A 10 ms cathodal S1 pulse was applied at rest to stimulate a propagated action potential. The pulse intensity was usually 1.5× the cathodal diastolic threshold (CDT). A 10-ms S2 pulse at 10× CDT was then applied with either anodal or cathodal polarity through the same electrode 100 ms after the S1 pulse. To check further the results obtained under these conditions, additional experiments were performed on hearts treated with a

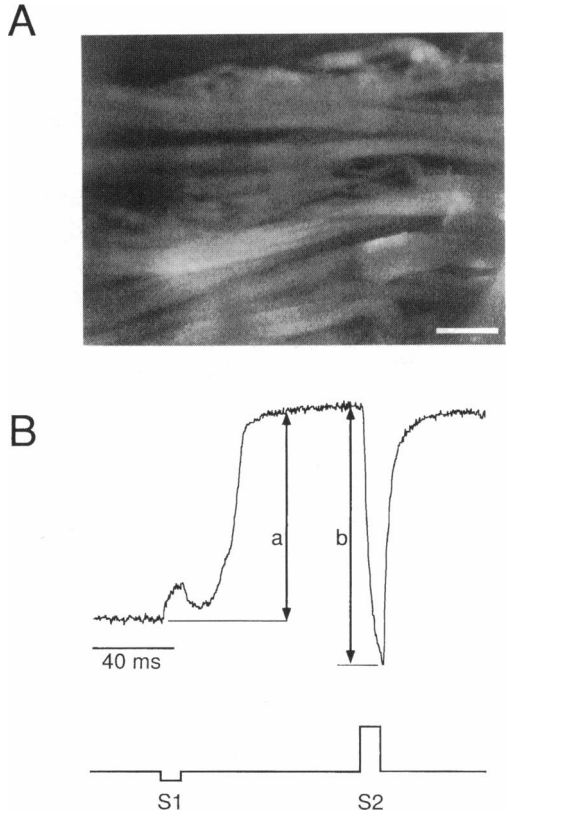

FIGURE 2 Experimental preparation and stimulation protocol of the bullfrog atrium. *A*, Fluorescence photomicrograph illustrating a region of the bullfrog endocardium. The image was obtained from an epifluorescence microscope with a 4× objective. The calibration mark is 300 μm. *B*, Illustration of the stimulation protocol. A cathodal S1 pulse at ~1.5× cathodal diastolic threshold (CDT) is applied to elicit a propagated action potential. 100 ms later an anodal S2 pulse (10× CDT in amplitude) is applied. The induced v_m is measured as the difference in membrane potential from the beginning of the pulse to the end of the pulse (*b*), normalized to the amplitude of the action potential (*a*). This trace was recorded adjacent to the stimulating electrode at a sampling frequency of 3 kHz.

number of channel blockers. S1 pulses at 10× CDT were applied to the preparation, where the CDT was determined prior to the application of the drug in the bath solution.

Measurement of V_m

The fractional change in fluorescence, $\Delta F/F$, is a measure of V_m (Salama, 1988). From this point on, the notation v_m will be used to indicate the change in transmembrane potential induced by the S2 pulse, measured as the value of $\Delta F/F$ at the end of the pulse relative to $\Delta F/F$ in the absence of the pulse. In this study, because the S2 pulse was applied during the ARP where the slope of the action potential is near zero, it was simpler and nearly equivalent to measure v_m as the change in $\Delta F/F$ from the beginning of the pulse to the end of the pulse. Because the magnitude of $\Delta F/F$ can vary slightly from site to site, $\Delta F/F$ was normalized to the value corresponding to the action potential amplitude (measured 50 ms after its upstroke; Fig. 2 *B*). The term "depolarization" will be used freely to mean positive v_m, and "hyperpolarization" to mean negative v_m.

Solutions and drugs

Standard Ringer solution consisted of (in mM) 110 NaCl, 3 KCl, 10 HEPES, 0.5 $CaCl_2$, pH = 7.3–7.4. A lowered Ca concentration was used to decrease the extent of tissue contraction and motion artifacts and does not significantly alter membrane conductance (Goldman and Morad, 1977). In one series of experiments, channel blockers were added to the Ringer solution: 10 μM TTX to block the Na channel, 5 mM 4-aminopyridine to block transient outward K channels, 20 mM TEA to block delayed rectifier K and K(Ca) channels, 1 mM $BaCl_2$ to block inward rectifier K channels, 1 mM $CdCl_2$ to block L-type Ca channels, and 1 mM $NiCl_2$ to block Na–Ca exchange current.

Statistical methods and curve fitting

Values are given as mean ± standard deviation. Data were analyzed statistically by the paired t-test. Values of $p < 0.05$ were considered to be significant. Data for v_m were fitted with a generalized curve-fitting routine contained in kaleidagraph (Synergy Software, Reading, PA).

Computer model

To assist in the interpretation of our experimental results, we formulated a computer model to describe the spatial distribution of v_m around a circular electrode placed on the surface of a semi-infinite conductive medium and located a small distance above the population of cardiac fibers (oriented parallel to one another and to the surface). Our approach is similar but not identical to that used by Rattay (1986, 1988) and Warman et al. (1992) to describe the response of a nerve fiber to extracellular stimulation.

When a step in voltage $V_o u(t)$ is applied to a metal disk electrode located (at the origin) on the surface of a semi-infinite isotropic volume conductor, the potential V_e at coordinates (x, y) in a plane a distance of z_o parallel to the surface is given by

$$V_e(r,t) = \frac{2V_o}{\pi}\sin^{-1}\left\{\frac{2a}{[(r-a)^2+z_o^2]^{1/2}+[(r+a)^2+z_o^2]^{1/2}}\right\}u(t), \quad (1)$$

where a is the electrode radius, $r = \sqrt{x^2+y^2}$, and $u(t)$ is the unit step function. The coefficient of $u(t)$ in Eq. 1 was derived by Wiley and Webster (1982) for the steady state, but this is quickly reached on a time scale of microseconds following the make of the stimulus pulse (inasmuch as reactive components of the tissue impedance are negligible). We also note that an equipotential surface is assumed at the tip of the electrode, which is only approximately true for our liquid-filled stimulating electrode. A key assumption in our model is that Eq. 1, which was derived for a monodomain, is an approximate description of the extracellular potential arising from an electrode placed on a bidomain. Indeed, it has been shown that for extracellular current injection into a two-dimensional bidomain, the extracellular potential is qualitatively similar to that expected for a monodomain (Sepulveda et al., 1989). Finally, the extracellular domain is generally anisotropic, whereas Eq. 1 is the solution to an isotropic medium. Even so, Eq. 1 should be approximately valid near the electrode surface (where V_e is large) because of the circular equipotential boundary condition imposed by the electrode.

A precise solution of the transmembrane potential of a cardiac fiber induced by an extracellular point electrode can be obtained through the use of frequency domain techniques and Laplace's equation applied to the intracellular and extracellular space (Altman and Plonsey, 1988). A simpler approach utilizing the so-called "activating function" will be used here to determine the qualitative behavior of v_m. The activating function has been described to be the equivalent bioelectric source that drives the changes in transmembrane potential of excitable fibers during extracellular field stimulation (Rattay, 1986). There are numerous limitations to such an approach: perturbations in extracellular field caused by the cardiac fibers are ignored, as are the transverse coupling between fibers, variation in extracellular potential around the circumference of the fibers, active membrane properties, and homogeneous solutions resulting from secondary sources (Altman and Plonsey, 1990). Recognizing these limitations but treating them as second-order effects during the S2 pulse, we intend to use our model primarily as a framework for the interpretation and discussion of our experimental results in terms of the activating function and other relevant parameters such as potential gradient.

We begin by considering the limiting case of the two-dimensional anisotropic bidomain model where the transverse intracellular conductivity is zero and the membrane is assumed to be passive and linear. The coordinate system is such that x is the longitudinal fiber direction and y the transverse fiber direction (Fig. 1). Under steady-state conditions, Roth (1992; Eq. 12) has shown that v_m satisfies the following one-dimensional cable equation:

$$\left(\frac{\sigma_{ex}R_m}{\beta}\right)\frac{\partial^2 v_m}{\partial x^2} - \frac{1}{\alpha}v_m = -\left(\frac{\sigma_{ex}R_m}{\beta}\right)S - \frac{1}{\alpha}\gamma_i, \quad (2)$$

where γ_i is any externally applied intracellular current, R_m is the specific membrane resistance, and σ_{ix}, σ_{iy}, σ_{ex}, and σ_{ey} are the conductivities in the intracellular and extracellular domains and x and y directions, respectively. Because σ_{iy} has been assumed to be zero, it, as well as the term σ_{ey} does not appear in Eq. 2. The parameter α is the ratio of intracellular and extracellular conductivities in the longitudinal fiber direction (σ_{ix}/σ_{ex}), and β is the ratio of membrane surface area to tissue volume. S is the "activating function," given by

$$S(x, t) = \frac{\partial^2 V_e}{\partial x^2}. \quad (3)$$

Generalizing the transmembrane current I_m to include capacitive and active components,

$$I_m = \beta\left(C_m\frac{\partial v_m}{\partial t} + \frac{v_m}{R_m} + I_m^a\right), \quad (4)$$

where C_m and I_m^a are the specific membrane capacitance and the active membrane current, Eq. 2 becomes

$$\lambda^2\frac{\partial^2 v_m}{\partial x^2} - \tau_m\frac{\partial v_m}{\partial t} - v_m = -\lambda^2 S + R_m I_m^a - \gamma_i, \quad (5)$$

where $\lambda = \sqrt{\sigma_{ix}R_m/\beta}$ and $\tau_m = R_m C_m$ are the fiber space constant and the membrane time constant, respectively.

Equation 5 may be better recognized in the form of the passive linear cable equation used to characterize nerve fibers:

$$\lambda^2\frac{\partial^2 v_m}{\partial x^2} - \tau_m\frac{\partial v_m}{\partial t} - v_m = r_e\lambda^2 I_{es} - r_i\lambda^2 I_{is}, \quad (6)$$

where r_e and r_i are the extracellular and intracellular resistances per unit length, respectively, and I_{es} and I_{is} are the externally applied, extracellular and intracellular current sources (if any). Equation 6 has a well-known solution for a step of source current of strength I_o located at an extracellular point on the fiber surface, i.e., for $I_{es} = I_o\,u(t)\delta(x)$, where $\delta(x)$ is the spatial delta function. The step response is given by (Plonsey and Barr, 1988)

$$v_m^s(x, t) = -r_e\lambda I_o\,W(x, t), \quad (7)$$

where

$$W(x, t) = W(X, T) = \frac{1}{4}\left[e^{-X}\mathrm{erfc}\left(\frac{X}{2\sqrt{T}} - \sqrt{T}\right) - e^{X}\mathrm{erfc}\left(\frac{X}{2\sqrt{T}} + \sqrt{T}\right)\right]u(t) \quad (8)$$

and X ($=x/\lambda$) and T ($=t/\tau_m$) are the dimensionless spatial and temporal variables. Comparing Eqs. 5 and 6 and neglecting intracellular and active membrane current sources (i.e., γ_i, I_m^a, and I_{is} are zero), it is clear that the activating function $S(x, t)$ behaves as an extracellular current source with strength I_o equal to $-S(x, t)/r_e$. Because $S(x, t)$ also can be considered to be an infinite sum of point sources, the total response of v_m to S is equal to the convolution of $S(x, t)$ and $\lambda W(x, t)$:

$$v_m(x,t) = \lambda\int S(\xi,t)W(x - \xi,t)\mathrm{d}\xi, \quad (9)$$

where ξ is the integration variable along the x axis. Equation 9 describes the step response of v_m at any point along the fiber during the stimulus pulse and shows clearly that $W(x, t)$ is a time-varying transfer function relating $v_m(x, t)$ to $S(x, t)$. The decay of v_m following the break of the stimulus pulse can easily be obtained by superposing upon Eq. 9 the solution to a second current step equal in magnitude but opposite in sign to the initial step and delayed in time by the pulse duration d. Thus, for $t \geq d$,

$$v_m(x, t) = \lambda\int S(\xi, t)W(x - \xi, t)\mathrm{d}\xi - \lambda\int S(\xi, t - d)W(x - \xi, t - d)\mathrm{d}\xi. \quad (10)$$

Equations 9 and 10 were implemented with MATLAB (MathWorks, Natick, MA) running on a Power Macintosh computer (Model 6100/60, Apple Computer, Cupertino, CA). Potentials were calculated over a region of $x = \pm 2$ mm and $y = 0$–2.4 mm, discretized in increments of 2 μm in the x direction and of 0.1 mm in the y direction. A distance of z_o in the range of 150–250 mm was assumed between the fiber and the electrode. The potential gradient in the x direction, $\nabla_x V_e$, and activating function S were calculated from V_e by mathematica (Wolfram Research, Champaign, IL).

RESULTS

We used a total of six bullfrog atria to measure the spatial distributions of v_m in two directions: one parallel ($n = 9$) and the other perpendicular ($n = 7$) to the fibers. In some cases multiple experiments were conducted on the same heart, in which case a new site was selected for the stimulating electrode for each experiment. The optical fiber was usually positioned in increments of 125 μm away from the electrode rim over a distance of 2.5 mm. As the recording distance from the stimulating electrode increased, there was an increased delay in the onset of the action potential associated with propagation (usually from 10 to 50 ms over 2.5 mm). Therefore, because the S1–S2 coupling interval was kept constant, the S2 pulse occurred earlier in the ARP as the recording site was moved farther away from the electrode. To check whether this factor could account for differences observed in v_m with distance from the stimulating electrode, on one occasion we measured v_m induced by anodal and cathodal S2 when S1–S2 was varied from 40 to 160 ms. The results showed that variation of S1–S2 interval over this range did not greatly affect the magnitude of v_m (variation of ± 0.016 from mean of 0.124 for cathodal pulses and ± 0.042 from -0.541 for anodal pulses).

v_m measured in the longitudinal fiber direction

The spatial distributions of v_m along the fiber axis are illustrated in Fig. 3 *A* for both cathodal and anodal S2 pulses. Two regions of opposite polarity coexist along the fiber. In a region delimited by the external rim of the electrode and a crossover point, v_m was depolarized for a cathode and hyperpolarized for an anode. Values of the parameters characterizing the longitudinal spatial distributions are summarized in Table 1. v_m measured adjacent to the electrode was always smaller with cathodal pulses than with equal amplitude anodal pulses (mean factor of 0.31, $p < 0.0005$, $n = 9$). The crossover point is defined as the location where $v_m = 0$ and reverses sign as defined by a polynomial curve fit of the data points. The crossover point depends on the pulse polarity (Fig. 3 *A*) and is significantly closer to the electrode for cathodal pulses than for anodal pulses (mean difference of 171 μm, $p < 0.0002$, $n = 9$). In the reversed polarity region, v_m increases in magnitude from the crossover point to a position where it reaches a maximum, which is significantly closer for cathodal pulses than for anodal pulses (mean

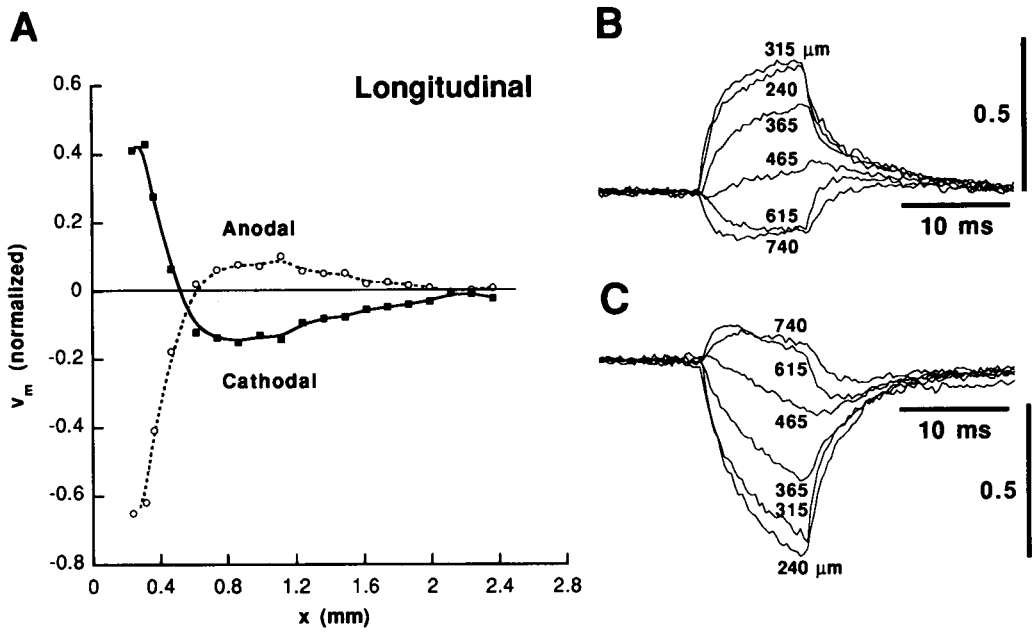

FIGURE 3 Recording obtained in the longitudinal fiber direction. The parameter v_m was measured at the end of a 10-ms S2 monophasic constant current pulse at 10× CDT for cathodal and anodal pulse polarities and normalized to the action potential amplitude. The numbers in *B* and *C* and the abscissa in *A* refer to distance of the recording site (center of the optical fiber) from the center of the stimulating electrode. *A*, Spatial distribution of v_m induced by the anode (- - - - -) and the cathode (——). A primary response exists in the region directly adjacent to the electrode, which reverses polarity as distance from the electrode increases. The crossover point between the two regions of polarity is closer to the electrode for cathodal pulses than for anodal pulses. In addition, the amplitude of the secondary, reversed polarized region is larger for cathodal pulses than for anodal pulses. *B*, Time courses of v_m for cathodal S2 pulses. The responses are purely depolarized 240 to 365 μm from the electrode. At 615 and 740 μm, v_m is purely hyperpolarized. An initial transient hyperpolarization can be seen near the crossover point (465 μm). *C*, Time courses of v_m for anodal S2 pulses. The responses are purely hyperpolarized 240 to 365 μm from the electrode. At 615 and 740 μm, v_m is purely depolarized. An initial transient depolarization can be seen near the crossover point (465 μm).

difference of 56 μm, $p < 0.045$, $n = 8$). Beyond this point v_m then decays monotonically to zero over a distance of approximately 1.5–2 mm. In addition the maximal amplitude of v_m in this reversed polarity region is significantly smaller for anodal pulses than for cathodal pulses (mean factor of 0.46, $p < 0.006$, $n = 9$). The time course of v_m at various distances from the electrode is shown during stimulation by cathodal (Fig. 3 *B*) and anodal (Fig. 3 *C*) pulses. In both cases, v_m measured at 240, 315, and 365 μm decreases monotonically to zero, as expected from linear cable theory (Plonsey and Barr, 1988). However, near the crossover point v_m exhibits an initial hyperpolarization for cathodal pulses (Fig. 3 *B*, traces 465, 615, 740), and depolarization for anodal pulses (Fig. 3 *C*, traces 465, 615, 740). These initial responses increase in amplitude to a maximum as described above.

v_m measured in the transverse fiber direction

Fig. 4 A illustrates the spatial decay of v_m in the direction perpendicular to the fiber axis for both anodal and cathodal S2 pulses. A cathodal pulse induces a depolarization that decays monotonically with distance from the stimulating electrode (Fig. 4 *B*). Conversely, an anodal pulse results in a monotonically decaying hyperpolarization (Fig. 4 *C*). Values of the parameters characterizing the transverse spatial

TABLE 1 Summary of spatial distributions of v_m along the longitidinal and transverse fiber axes[a]

	Cathode	Anode	*p*
Longitudinal			
v_m adjacent to electrode	+0.262 ± 0.114	−0.832 ± 0.275	<0.0005, $n = 9$
x value for crossover	445 ± 112 μm	616 ± 78 μm	<0.0002, $n = 9$
Peak reversed v_m	−0.347 ± 0.194	+0.160 ± 0.160	<0.006, $n = 9$
x value for peak reversed v_m	922 ± 136 μm	978 ± 117 μm	<0.045, $n = 8$
Transverse			
v_m adjacent to electrode	0.628 ± 0.223	1.224 ± 0.566	<0.0045, $n = 7$
Spatial decay constant	343 ± 110 μm	253 ± 91 μm	<0.012, $n = 6$

[a] The distributions are characterized by the parameters indicated in the first column. The mean ± SD of each parameter measured for cathodal and anodal stimulation is shown. Values for v_m are normalized to the amplitude of the action potential. Test of the statistical significance of the difference in each parameter under cathodal and anodal stimulation was performed using a paired t-test, and the result shown in the fourth column together with the number of paired data points.

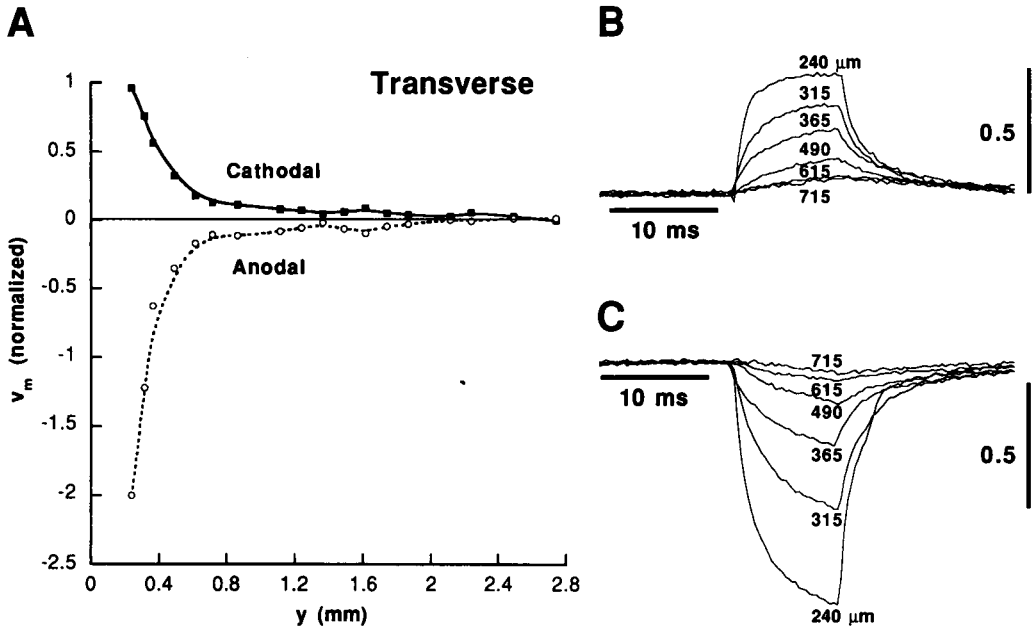

FIGURE 4 Recording obtained in the transverse fiber direction. The parameter v_m was measured at the end of a 10-ms S2 monophasic current pulse at 10× CDT for cathodal and anodal pulse polarities and normalized to the action potential amplitude (vertical calibration bars). The numbers in *B* and *C* and the abscissa in *A* refer to the distance of the recording site (center of the optical fiber) from the center of the stimulating electrode. *A*, Spatial distribution of v_m induced by anodal (- - - - -) and cathodal (——) pulses. The magnitude of v_m decays monotonically with distance from the electrode. *B*, Time courses of v_m for cathodal S2 pulses. *C*, Time courses of v_m for anodal S2 pulses.

distributions are summarized in Table 1. When a monoexponential function was used to fit the spatial decay of v_m, the decay constant was significantly larger for cathodal pulses than for anodal pulses (mean factor of 1.36, $p < 0.012$, $n = 6$). As observed in the longitudinal direction, v_m adjacent to the electrode was always smaller when induced by a cathodal pulse than an anodal one (mean factor of 0.51, $p < 0.0045$, $n = 7$). Comparing Fig. 4 *A* with Fig. 3 *A* shows that v_m adjacent to the electrode is larger in the transverse direction than in the longitudinal direction, for both cathodal and anodal pulses. Although the data shown were obtained from two different preparations, experiments in which both distributions were obtained from the same preparation, with the stimulus electrode at the same position and intensity ($n = 3$), confirm the larger v_m in the transverse direction. At distances greater than 1 mm from the electrode there is no longer a statistically measurable difference in responses for the two pulse polarities ($p < 0.2$). Fig. 4 *B* and *C* illustrate, respectively, the time course of v_m during cathodal and anodal S2 pulses. The traces measured at various distances from the electrode are superposed. We observe that for both cathodal and anodal pulses, the peak amplitude of v_m decreases with distance from the electrode. The time course of v_m follows a nearly exponential charging and discharging response during the pulse. We fitted v_m with a monoexponential function $\zeta = A[1 - \exp(-t/\tau)]$ over the pulse interval and in Fig. 5 plotted (+) or (−) $\ln[1 - (\zeta/A)]$ as a function of time for both pulse polarities. The plots are nearly linear over this time range with a slope proportional to $1/\tau$. For either pulse polarity, τ increases with increasing distance from the electrode. Furthermore, τ for a cathodal pulse is less than that for an anodal pulse with equal amplitude.

Response in the longitudinal and transverse fiber directions in the presence of channel blockers

To determine whether the previous observations were the result of intrinsic passive cable properties of the tissue, we bathed the heart in Ringer solution containing various channel blockers as described in the Materials and Methods section. In this series of measurements no action potential could be elicited, so v_m was elicited by S1 pulses and expressed directly as $\Delta F/F$ (in units of percent) rather than as a parameter normalized to action potential amplitude. Although errors can result if the fraction of nonexcitable stained tissue that contributes to F but not to ΔF varies with the recording site, we did not find a significant difference in our previous results, at least for normal Ringer solution (Figs. 3 and 4) if v_m were measured in unnormalized as opposed to normalized units.

The results that we obtained under these conditions (Fig. 6) were qualitatively similar to those obtained in the absence of channel blockers (Figs. 3 and 4), supporting the conclusion that the spatial behavior of v_m is an inherent passive property of cardiac muscle. In the longitudinal direction ($n = 2$) and for cathodal pulses, a depolarized region results near the electrode and is accompanied by one hyperpolarized farther away (>400 μm) (Fig. 6 *A* and *B*). Conversely with anodal pulses, a hyperpolarized region near the anode coexists with one depolarized farther away (Fig. 6 *A* and *C*). However, com-

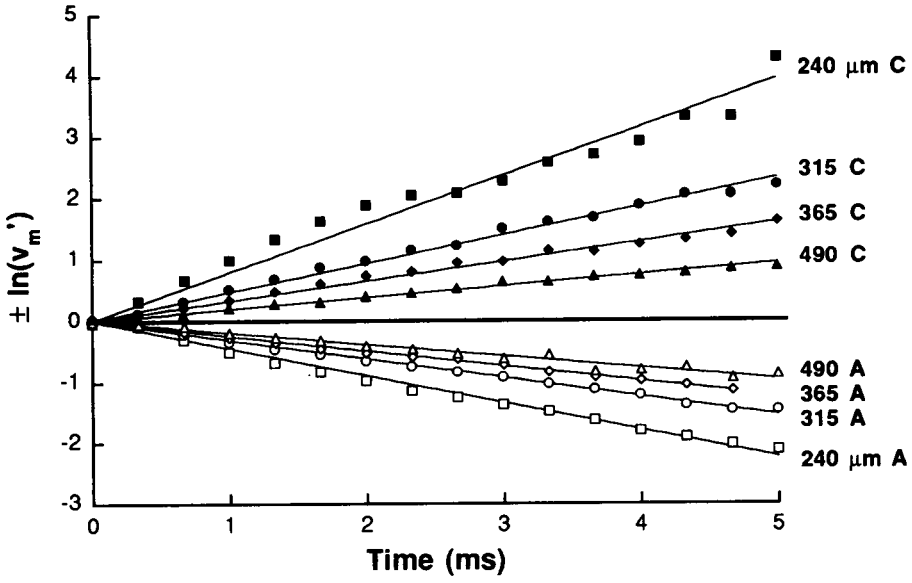

FIGURE 5 Plot of the data of Fig. 4, illustrating the change in membrane time constant of v_m as the distance from the stimulating electrode increases. Plotted is $-\ln(v_m')$ for cathodal pulses and $\ln(v_m')$ for anodal pulses as a function of time, where v_m' is defined as $1 - (v_m/A)$ and A is obtained as a parameter for the best-fit exponential function of the form $A[1 - \exp(-t/\tau)]$. The function is linear over the first 5 ms of the S2 pulse and has a slope inversely proportional to the membrane time constant. The numbers refer to distance from the center of the stimulating electrode, C to cathodal pulse, and A to anodal pulse.

pared with the case without channel blockers, for this case the crossover points occur at distances closer to the electrode, and the peak amplitude of v_m in the reversed polarity region is comparable with that measured immediately adjacent to the electrode (compare Fig. 6 *A* with Fig. 3 *A*).

In the transverse direction ($n = 2$), the spatial distributions of v_m are purely depolarized for cathodal pulses (Fig. 6 *D* and *E*) and hyperpolarized for anodal pulses (Fig. 6 *D* and *F*) and are very similar to those obtained in the absence of channel blockers. The amplitude of v_m is smaller for cathodal pulses than for anodal pulses, suggesting that some nonlinear channel conductance remains. An analysis of the time courses of v_m for both cathodal and anodal pulses, similar to that of Fig. 5, shows an increase in time constant with increasing distance from the electrode, as was observed in the case without channel blockers.

Model predictions

The spatial distributions predicted by our model of extracellular potential V_e, extracellular potential gradient $\nabla_x V_e$ ($=\partial V_e/\partial x$), activating function S, and transmembrane potential v_m are shown in the longitudinal fiber direction in Fig. 7. V_e is maximum in amplitude at $x = 0$ and decays monotonically to zero. $\nabla_x V_e$ reaches a maximum at $x = 0.46\lambda$ and has a single polarity along x. S is maximum at $x = 0$ and reverses polarity at $x = 0.46\lambda$. v_m has a shape similar to that of S but is extended out along x and reverses polarity at $x = 0.85\lambda$.

To test the predictions of the model, we used the experimental data of Figs. 3 *A* and 4 *A* obtained during cathodal stimulation (showing the spatial distributions of v_m in the longitudinal and transverse directions at the end of the S2 pulse) to attempt a model fit. The results are shown in Fig. 8 *A* and *B*, where the ordinate has been normalized to the action potential amplitude rather than the peak amplitude at $x = 0$ (which is unknown). Reasonably good fits were obtained, with reasonable values for the model parameters. The differing amplitudes of the fits in the longitudinal and transverse directions at $x = 0$ may be due to uncontrolled differences in distances from fiber to electrode (z_o) in the two experiments.

Fig. 9 *A* and *B* shows the model predictions of the time courses of v_m during a cathodal S2 pulse, at various sites along the longitudinal and transverse directions. At all sites the time course only approximates, but is not strictly, an exponential, as expected from Eqs. 7 and 8. Over a limited time interval, however, an "apparent" time constant can be computed by fitting a monoexponential function. In the longitudinal direction, responses of both polarities can be observed at $x = 0.2\lambda$ and $x = 2\lambda$, with a slower time constant for the response at 0.2λ. This behavior is seen in the experimental traces of Fig. 3 *B*. In the transverse direction, the responses are all of a single polarity. Analysis of apparent time constants (τ) during the time interval $0 \leq t \leq \tau_m$ (Fig. 9 *B*), similar to that used for Fig. 5, shows that τ increases with distance from the electrode ($\tau = 0.16\ \tau_m$, $0.21\ \tau_m$, $0.42\ \tau_m$ at $x = 0.2\lambda$, 0.4λ, 2λ, respectively), which is qualitatively similar to the experimental observations of Fig. 5.

Finally, the model predictions of the complete two-dimensional spatial profiles of v_m are shown as equipotential contour maps in Fig. 10, which are a function of time following the make of the cathodal S2 pulse. At short times ($t = 0.1\tau$), a primary region of depolarization with an elliptical shape is observed near the stimulating electrode, with the long axis oriented in the transverse fiber direction (a secondary region with elliptical shape and reversed polarity exists along the longitudinal axis but is very small in amplitude and therefore does not appear). With time, the primary region takes on a dog-bone shape, and the reversed polarity region gains amplitude. The contour map shown at $t = 5\tau$ is nearly that obtained at steady state.

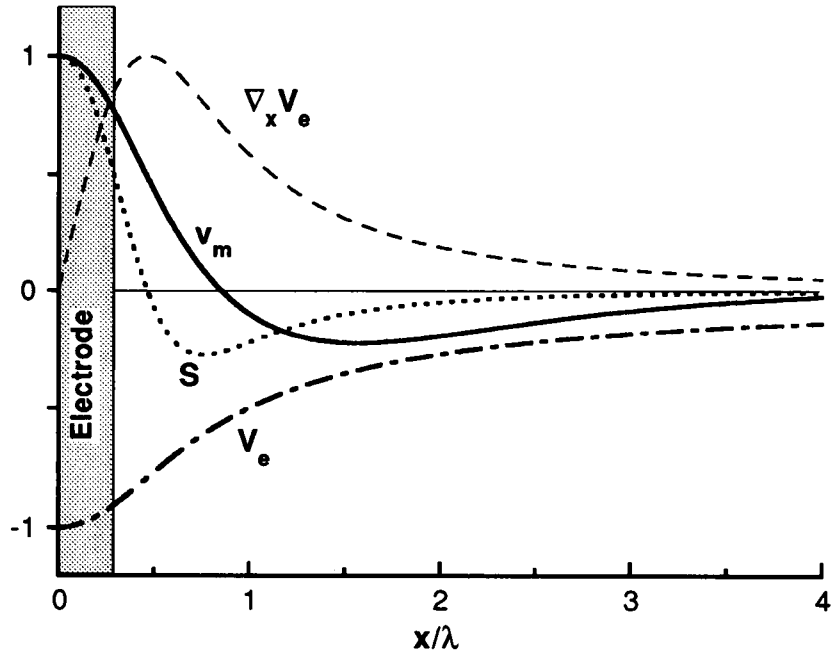

FIGURE 7 Spatial distributions of extracellular potential, potential gradient, activating function, and membrane potential induced by cathodal pulses. A pulse duration of 10 ms was assumed, at the end of which the spatial distributions were calculated. The extracellular potential V_e (– · – · –), potential gradient $\nabla_x V_e = \partial V_e/\partial x$ (- - - -), activating function S (· · · · ·), and membrane potential v_m (——) are plotted as functions of radial distance x from the center of the stimulating electrode. The stimulating voltage V_0 was set to 1.5 V in this simulation, the electrode diameter a to 0.3λ, the electrode elevation z_0 to 0.5λ, and the space constant λ to 500 μm. The four curves have been normalized to their peak values (0.52 V, 7 V/cm, 496 V/cm^2, and 82.7 mV, respectively).

DISCUSSION

Although theoretical models have been developed recently to describe the influence of fiber direction on changes in v_m around a unipolar stimulating electrode, experimental studies addressing these issues have been limited in number. Previous work from our laboratory has shown the presence of reversed polarized regions (i.e., opposite polarity, virtual electrode) that coexist around an extracellular electrode (Neunlist and Tung, 1992; Neunlist and Tung, 1994a; Tung et al., 1994). In those studies the pattern of polarization could not be clearly discerned, because the fiber orientations in the preparations that were used (frog ventricle) were not well defined. In this study v_m was measured in both the longitudinal and the transverse directions of trabeculae bundles in the bullfrog atrium, where the fiber orientation is clear (Fig. 2). The major finding is that secondary, reversed polarity regions appear during stimulation that are located along the longitudinal and not the transverse fiber direction and behave as a virtual electrode with polarity opposite that of the stimulating electrode. Our experimental observations remain qualitatively the same with the addition of channel blockers to the tissue, suggesting that the observed behavior arises from the passive (and structurally related) electrical properties of the myocardium.

Recently, Knisley et al. (1994) reported virtual electrode effects in the rabbit ventricle similar to those described here: 1) sites along one direction next to a point electrode, having reversed polarity from a linear cable response, 2) regions of tissue having reversed polarity adjacent and parallel to a linear electrode array, and 3) responses of v_m to cathodal S2 pulses that were larger than those for anodal pulses. Fiber direction was inferred from conduction velocity measurements, and no data were obtained in the orthogonal direction. In contrast to their study, we identified fiber direction by direct anatomical observation (Fig. 2 *A*). Our recordings of v_m were obtained at a high spatial resolution and extend close to the electrode. Thus, the complementary regions of polarity (and crossover point) along the longitudinal fiber direction are clearly delimited (Figs. 3 *A* and 6 *A*). Most importantly, as a test of the theory, we measured the distribution of v_m in both the longitudinal and the transverse fiber directions (Figs. 3 *A* and 4 *A*).

The model that we have presented here provides a reasonably good fit to the experimental measurements of the spatial and temporal variations in v_m (Figs. 8 and 9), despite the many limitations of the approach iterated above. The model reproduces the spatial behavior of v_m around the stimulating electrode, showing coexisting, oppositely polarized regions in the longitudinal direction and a monotonically decaying polarized region in the transverse direction. Near the electrode, v_m is larger in the transverse direction than in the longitudinal direction (Fig. 10), as was observed (Figs. 3 *A* and 4 *A*). As expected, the activating function S is only a qualitative approximation of the spatial distribution of v_m in the two directions, the latter appearing to be a spatially low-pass filtered version of S (Fig. 7). We see from Eq. 9 and Fig. 10 the basis for the difference between v_m and S. At early times during the S2 pulse ($t = 0.1\tau$), v_m mimics the activating function S, because the transfer function $W(x, t)$ is nearly a delta function in space. However, with time, charge spreads down the axis of the fibers as $W(x, t)$ widens. This results in the migration of equipotential contour lines away from the stimulating electrode ($t = 0.5\tau$, τ, 5τ). A similar time-dependent evolution of contour plots has been predicted by Roth and Trayanova (1993). The same phenomenon underlies the time-dependent changes in v_m measured at various points in space (Fig. 9). For example, v_m measured near the crossover point undergoes a biphasic behavior. The initial

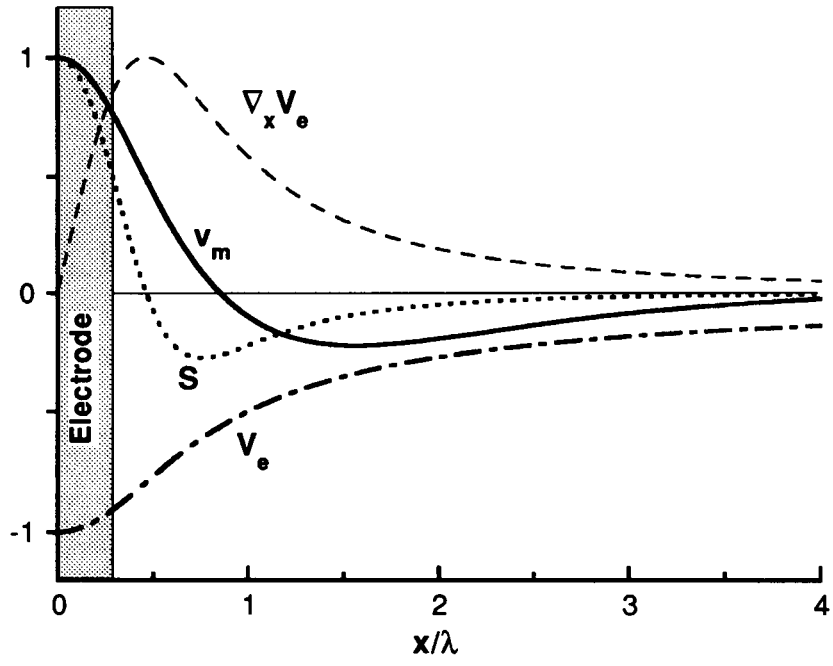

FIGURE 7 Spatial distributions of extracellular potential, potential gradient, activating function, and membrane potential induced by cathodal pulses. A pulse duration of 10 ms was assumed, at the end of which the spatial distributions were calculated. The extracellular potential V_e (– · – · –), potential gradient $\nabla_x V_e = \partial V_e/\partial x$ (- - - -), activating function S (· · · · ·), and membrane potential v_m (——) are plotted as functions of radial distance x from the center of the stimulating electrode. The stimulating voltage V_0 was set to 1.5 V in this simulation, the electrode diameter a to 0.3λ, the electrode elevation z_0 to 0.5λ, and the space constant λ to 500 μm. The four curves have been normalized to their peak values (0.52 V, 7 V/cm, 496 V/cm^2, and 82.7 mV, respectively).

DISCUSSION

Although theoretical models have been developed recently to describe the influence of fiber direction on changes in v_m around a unipolar stimulating electrode, experimental studies addressing these issues have been limited in number. Previous work from our laboratory has shown the presence of reversed polarized regions (i.e., opposite polarity, virtual electrode) that coexist around an extracellular electrode (Neunlist and Tung, 1992; Neunlist and Tung, 1994a; Tung et al., 1994). In those studies the pattern of polarization could not be clearly discerned, because the fiber orientations in the preparations that were used (frog ventricle) were not well defined. In this study v_m was measured in both the longitudinal and the transverse directions of trabeculae bundles in the bullfrog atrium, where the fiber orientation is clear (Fig. 2). The major finding is that secondary, reversed polarity regions appear during stimulation that are located along the longitudinal and not the transverse fiber direction and behave as a virtual electrode with polarity opposite that of the stimulating electrode. Our experimental observations remain qualitatively the same with the addition of channel blockers to the tissue, suggesting that the observed behavior arises from the passive (and structurally related) electrical properties of the myocardium.

Recently, Knisley et al. (1994) reported virtual electrode effects in the rabbit ventricle similar to those described here: 1) sites along one direction next to a point electrode, having reversed polarity from a linear cable response, 2) regions of tissue having reversed polarity adjacent and parallel to a linear electrode array, and 3) responses of v_m to cathodal S2 pulses that were larger than those for anodal pulses. Fiber direction was inferred from conduction velocity measurements, and no data were obtained in the orthogonal direction. In contrast to their study, we identified fiber direction by direct anatomical observation (Fig. 2 *A*). Our recordings of v_m were obtained at a high spatial resolution and extend close to the electrode. Thus, the complementary regions of polarity (and crossover point) along the longitudinal fiber direction are clearly delimited (Figs. 3 *A* and 6 *A*). Most importantly, as a test of the theory, we measured the distribution of v_m in both the longitudinal and the transverse fiber directions (Figs. 3 *A* and 4 *A*).

The model that we have presented here provides a reasonably good fit to the experimental measurements of the spatial and temporal variations in v_m (Figs. 8 and 9), despite the many limitations of the approach iterated above. The model reproduces the spatial behavior of v_m around the stimulating electrode, showing coexisting, oppositely polarized regions in the longitudinal direction and a monotonically decaying polarized region in the transverse direction. Near the electrode, v_m is larger in the transverse direction than in the longitudinal direction (Fig. 10), as was observed (Figs. 3 *A* and 4 *A*). As expected, the activating function S is only a qualitative approximation of the spatial distribution of v_m in the two directions, the latter appearing to be a spatially low-pass filtered version of S (Fig. 7). We see from Eq. 9 and Fig. 10 the basis for the difference between v_m and S. At early times during the S2 pulse ($t = 0.1\tau$), v_m mimics the activating function S, because the transfer function $W(x, t)$ is nearly a delta function in space. However, with time, charge spreads down the axis of the fibers as $W(x, t)$ widens. This results in the migration of equipotential contour lines away from the stimulating electrode ($t = 0.5\tau$, τ, 5τ). A similar time-dependent evolution of contour plots has been predicted by Roth and Trayanova (1993). The same phenomenon underlies the time-dependent changes in v_m measured at various points in space (Fig. 9). For example, v_m measured near the crossover point undergoes a biphasic behavior. The initial

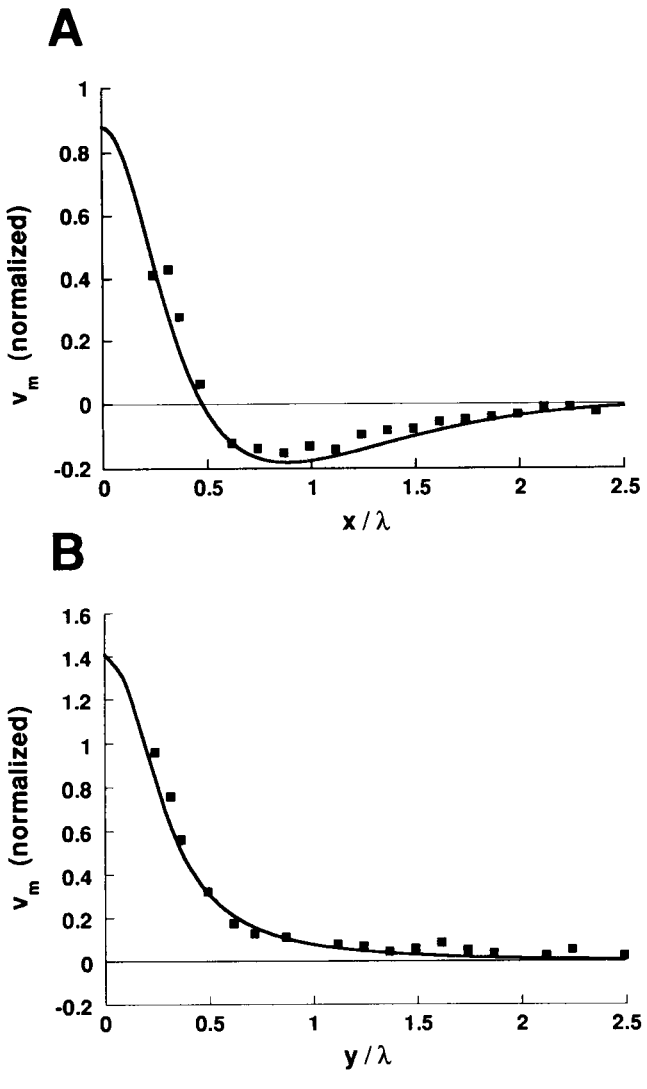

FIGURE 8 Model predictions and fit of the experimentally measured distributions of v_m induced by cathodal pulses. The transmembrane potential response v_m is plotted as a function of distance from the center of the electrode along the longitudinal (*A*) and transverse (*B*) fiber directions. Data are reproduced from Figs. 3 *A* and 4 *A* for cathodal stimulation, and the fit was determined by eye. The ordinate has been normalized to the action potential amplitude. For the simulations, the electrode radius a was assumed to be 0.25λ, the elevation z_0 to be 0.417λ in the longitudinal direction and 0.3λ in the transverse direction, the pulse duration to be 10 ms, the membrane time constant τ to be 14 ms, and tissue space constant λ to be 600 μm.

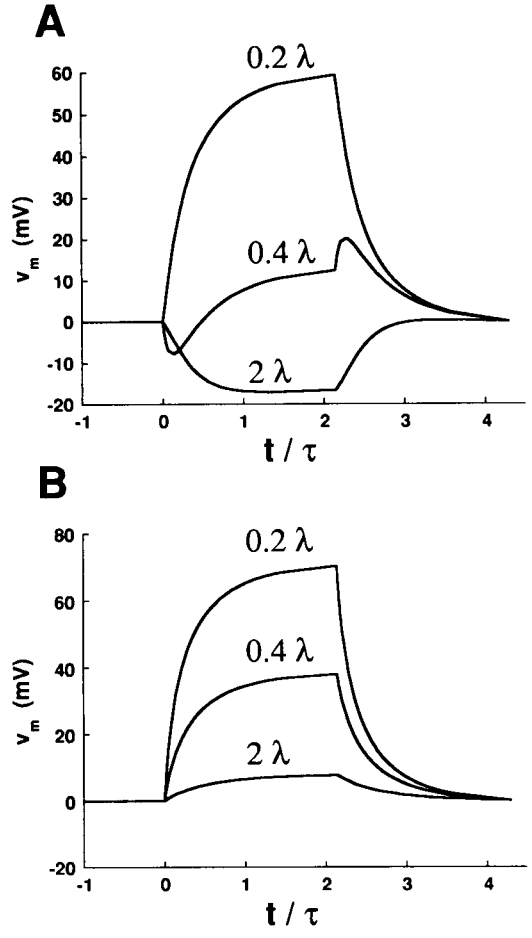

FIGURE 9 Model predictions of the temporal responses of v_m induced by cathodal pulses. In this simulation, the stimulus pulse was given a duration of 5τ so that v_m reached near-steady-state conditions at the end of the pulse. The electrode radius a was assumed to be 0.3λ and the elevation z_0 to be 0.5λ. The responses for v_m "measured" at distances of 0.2, 0.4, and 2λ from the center of the stimulating electrode are plotted along the longitudinal (*A*) and transverse (*B*) directions.

transient hyperpolarization accompanying the cathodal S2 pulse (Fig. 3 *B*, trace 465) results from the virtual anode generated along the longitudinal axis. With time, the region of the virtual anode migrates away from the electrode, so that the recording site becomes depolarized. Our model also reproduces the different time courses observed as the distance from the stimulating electrode increases. In the longitudinal direction (Fig. 9 *A*), v_m reaches steady state more rapidly in the secondary, reversed polarity region (x = 2λ) than in the primary polarity region (x = 0.2λ), as observed experimentally in Fig. 3 *B*. In the transverse direction (Fig. 9 *B*), the time course of v_m is slower at distances farther from the electrode, as observed experimentally in Fig. 4 *B*.

Passive linear models of anisotropic cardiac muscle (Sepulveda et al., 1989; Roth, 1992; Roth and Trayanova, 1993), including the model presented here, predict distributions of v_m that are symmetric in amplitude with stimulus polarity, with identical crossover points of v_m in the longitudinal direction. In our experiments, the distribution of v_m is not symmetric in amplitude for cathodal and anodal pulses, nor are the crossover points identical (Fig. 3 *A*). Therefore the asymmetry in v_m for anodal and cathodal pulses (with larger response for anodal pulses; Figs. 3 and 4) can be attributed to a voltage-dependent membrane conductance together with active membrane currents. Indeed, it is known that the membrane conductance rectifies in the outward direction during the ARP with a lower resistance during depolarization (Goldman and Morad, 1977), which would be consistent with our results. It also is known that, at rest, the membrane conductance rectifies in the inward direction, in which case we would predict an asymmetry with pulse polarity for pulses applied at rest but with v_m larger for cathodal rather than anodal pulses. In previous studies we observed

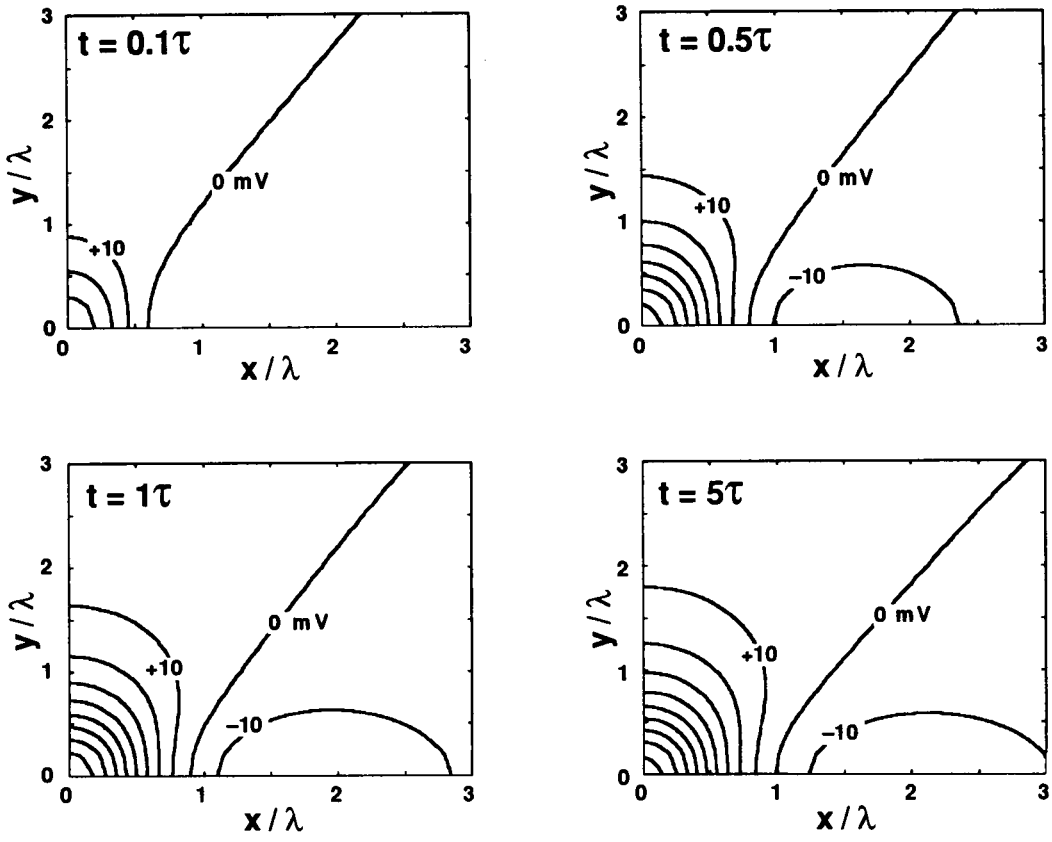

FIGURE 10 Evolution of the two-dimensional spatial distributions of v_m following the make of a rectangular, cathodal stimulus pulse. The conditions for this simulation were identical to those of Fig. 9. Because of biaxial symmetry of the responses in space, only one quadrant is shown. Isopotential contours for v_m are plotted at 10-mV intervals. Immediately following the make of the pulse ($t = 0.1\tau$), the isopotential contours are nearly elliptical, with the major axis aligned in the transverse direction. At $t = 0.5\tau$, formation of a focal region of hyperpolarization can be observed on the longitudinal axis, centered at ~1.6λ. At $t = \tau$, the isopotential contours form a distinct dog-bone shape with positive polarity along the transverse direction, and elliptical shapes with negative polarity along the longitudinal direction. At $t = 5\tau$, the isopotential contours have migrated farther away from the electrode in both the longitudinal and transverse directions, nearly to their steady-state positions. Because a linear membrane was assumed in our model, the identical contour plots would be obtained, but with reversed polarity, for an anodal stimulus pulse of equal amplitude.

such an asymmetry to be the case (Tung et al., 1991; Neunlist and Tung, 1994a). That voltage-dependent changes in membrane conductance influence the amplitude of v_m is not unexpected, because λ and τ are then altered, in turn altering $W(x, t)$, the transfer function from S to v_m (cf. Eq. 8). Therefore the amplitude and the spatial extent of the oppositely polarized, virtual electrode regions may be influenced by the timing of the S2 pulse in the action potential during which time membrane conductance varies. Active membrane currents, which also are not accounted for in our model, can influence the spatial and temporal patterns of v_m in the form of source terms on the right-hand side of Eq. 5. Consistent with this hypothesis, when ionic channel blockers are applied the spatial and temporal patterns of v_m are altered (compare Fig. 6 with Figs. 3 and 4), although the qualitative behavior is preserved.

Our model shows that, even in the absence of transverse coupling, v_m decays in approximately an exponential fashion in the transverse fiber direction (as observed in Fig. 4 *A*) as a consequence of the spatial decay of the activating function. The slower rise time of v_m with increasing distance from the electrode (as observed in Fig. 5) also is predicted by our model. We consider now the effect of transverse coupling. It has been shown that up to the point where the anisotropy of the intracellular domain equals that of the extracellular domain (i.e., $\sigma_{iy}/\sigma_{ix} = \sigma_{ey}/\sigma_{ex}$), the effect of increasing the intracellular transverse conductance (σ_{iy}) from zero is to decrease the amplitude of the reversed polarity region and to shift the region in the longitudinal direction away from the electrode (Sepulveda et al., 1989; Roth, 1992) (increasing transverse conductance beyond this point would create a reversed polarity region along the transverse and not the longitudinal direction, but this case is unphysiological). However, the spatial distributions along the two fiber axes would remain qualitatively the same. Therefore, our results do not exclude transverse coupling. In future studies, it may be possible to determine the transverse coupling quantitatively using off-axis measurements of v_m, because it has been shown theoretically that the shape of the dog-bone and trajectory of the zero potential contour (Fig. 10) depend on this parameter (Sepulveda et al., 1989; Roth, 1992).

Our results showing oppositely polarized regions around a stimulating electrode differ from those of earlier experiments performed on rat atrial trabeculae (Woodbury and Crill, 1961) and mouse ventricle (Tanaka and Sasaki, 1966). In both studies, only a single polarity response was observed in both the longitudinal and transverse directions, with v_m decaying as a zero-order Bessel function of the second kind. One explanation for the difference in their results may be the mode of stimulation that was used. Both studies used an intracellular stimulating electrode, which, unlike the extracellular stimulating electrode that we used, does not generate an activating function or its consequence, a reversed polarity region along the longitudinal fiber axis. Another possibility is that the farthest site measured was at 500 μm, which may have fallen short of the crossover point if a secondary, oppositely polarized region in fact existed.

It has been suggested that the extracellular potential gradient is the critical parameter implicated in cardiac stimulation and defibrillation (Lepeschkin et al., 1978; Walcott et al., 1994). However, it is ultimately v_m that is involved. Our model shows that the magnitudes of v_m and $\nabla_x V_e$ ($=\partial V_e/\partial x$) are not well correlated over a range of distances in the longitudinal direction (Fig. 7). It is even possible for a given value of $\nabla_x V_e$ to be associated with transmembrane potentials of opposite polarity. For example, at $\nabla_x V_e = 0.5$ of the peak amplitude, $v_m = 0.93$ at $x = 0.15\lambda$ and -0.15 at 1.12λ. Furthermore, $\nabla_x V_e$ and v_m have different time courses. The extracellular potential gradient is instantaneously established with the pulse (and is constant during the pulse), whereas v_m evolves with time as a result of charge diffusion down the fiber axis (as shown in Fig. 10). Active transmembrane currents also will have differing influences on $\nabla_x V_e$ and v_m. Thus, our results suggest that caution should be taken when attempting to understand the membrane response solely in terms of potential gradient. On the other hand, it should be kept in mind that the tissue region described in this study is adjacent to the stimulating electrode. In regions far from the electrode where the contribution of the activating function may be low and of secondary sources may be high, a stronger correlation may exist between v_m and $\nabla_x V_e$ (Krassowska et al., 1990).

POSSIBLE IMPLICATIONS OF THIS STUDY

In a previous study we showed that anodal excitation during diastole is initiated in the frog ventricle by a reversed, depolarized region adjacent to the extracellular anode (Neunlist and Tung, 1994a). The recent work of Knisley et al. (1994) and Roth and Wikswo (1994) also supports this hypothesis. Our results show that, during stimulation with monophasic pulses, complementary regions of reversed membrane polarization coexist next to the stimulating electrode, regardless of the polarity of the stimulus pulse. For electrical pulses applied during the refractory period, those regions that are hyperpolarized can reactivate inactivated Na channels. Following the pulse, the adjacent regions of depolarization will electrotonically depolarize the hyperpolarized regions. If the Na channels have been sufficiently reprimed during the period of hyperpolarization, a new action potential now can be initiated. With anodal stimulation, the hyperpolarized region lies along the longitudinal direction over a short extent immediately adjacent to the electrode (Fig. 3 *A*) and extends in the transverse direction all along the axis (Fig. 4 *A*). On the other hand, with cathodal stimulation, the hyperpolarized region exists only as the secondary (virtual electrode) region along the longitudinal direction (Fig. 3 *A*), with a relatively low amplitude. These differences in regional size and amplitude of the hyperpolarized region are substantiated by our model (Fig. 10) and may well be responsible for the well-known greater efficacy of anodal pulses over cathodal pulses to stimulate during the relative refractory period (Cranefield et al., 1957).

In conclusion, this study correlates the pattern of v_m around an extracellular electrode with the local fiber orientation in the bullfrog atrium. Our findings show adjacent, oppositely polarized regions in the longitudinal fiber direction and a single polarized region in the transverse direction. The amplitude, extent, and temporal development of these regions depend on the fiber orientation, pulse polarity, membrane conductance, and active membrane currents. A simple anisotropic electrical model, based on the limiting case of the two-dimensional anisotropic bidomain model, qualitatively accounts for nearly all the observed spatial and temporal behavior of v_m along both fiber directions.

Note added in proof—While this article was in press, Plonsey and Barr (*IEEE Trans. Biomed. Eng.* 42:329–336, 1995) published a model for electric field stimulation using an approach similar to the one we have described here.

This work was supported by National Institutes of Health grant HL48266. We wish to thank Eric Sobie for his assistance in reviewing this manuscript and Bertram Lewis and Wei Guo for their assistance in the early part of the computational work.

REFERENCES

Altman, K. W., and R. Plonsey. 1988. Development of a model for point source electrical fibre bundle stimulation. *Med. Biol. Eng. Comput.* 26: 466–475.

Altman, K. W., and R. Plonsey. 1990. Analysis of excitable cell activation: relative effects of external electrical stimuli. *Med. Biol. Eng. Comput.* 28:574–580.

Chen, P.-S., Y.-M. Cha, B. B. Peters, and L. S. Chen. 1993. Effects of myocardial fiber orientation on the electrical induction of ventricular fibrillation. *Am. J. Physiol.* 264:H1760–H1773.

Cranefield, P. F., B. F. Hoffman, and A. A. Siebens. 1957. Anodal excitation of cardiac muscle. *Am. J. Physiol.* 190:383–390.

Dillon, S. M. 1992. Synchronized repolarization after defibrillation shocks. *Circulation.* 85:1865–1878.

Dillon, S. M., M. A. Allessie, P. C. Ursell, and A. L. Wit. 1988. Influences of anisotropic tissue structure on reentrant circuits in the epicardial border zone of subacute canine infarcts. *Circ. Res.* 63:182–206.

Dillon, S. M., and A. L. Wit. 1988. Use of voltage sensitive dyes to investigate electrical defibrillation. *Proc. Ann. Int. Conf. IEEE Eng. Med. Biol. Soc.* 10:215–216.

Frazier, D. W., W. Krassowska, P.-S. Chen, P. D. Wolf, E. G. Dixon, W. M. Smith, and R. E. Ideker. 1988. Extracellular field required for excitation in three dimensional anisotropic canine myocardium. *Circ. Res.* 63:147–164.

Goldman, Y., and M. Morad. 1977. Ionic membrane conductance during the time course of the cardiac action potential. *J. Physiol. (London).* 268: 655–695.

Henriquez, C. S. 1993. Simulating the electrical behavior of cardiac tissue using the bidomain model. *Crit. Rev. Biomed. Eng.* 21:1–77.

Knisley, S. B., T. F. Blitchington, B. C. Hill, A. O. Grant, W. M. Smith, T. C. Pilkington, and R. E. Ideker. 1993. Optical measurements of transmembrane potential changes during electric field stimulation. *Circ. Res.* 72:255–270.

Knisley, S. B., B. C. Hill, and R. E. Ideker. 1994. Virtual electrode effects in myocardial fibers. *Biophys. J.* 66:719–728.

Knisley, S. B., W. M. Smith, and R. E. Ideker. 1992. Effect of field stimulation on cellular repolarization in rabbit myocardium. *Circ. Res.* 70: 707–715.

Krassowska, W., C. Cabo, S. B. Knisley, and R. E. Ideker. 1992. Propagation versus delayed activation during field stimulation of cardiac muscle. *Pacing Clin. Electrophysiol.* 15:197–210.

Krassowska, W., D. W. Frazier, T. C. Pilkington, and R. E. Ideker. 1990. Potential distribution in three-dimensional periodic myocardium. Part II. Application to extracellular stimulation. *IEEE Trans. Biomed. Eng.* 37: 267–284.

Lepeschkin, E., J. L. Jones, S. Rush, and R. E. Jones. 1978. Local potential gradients as a unifying measure for threshold of stimulation, standstill, tachyarrhythmia, and fibrillation appearing after strong capacitor discharges. *Adv. Cardiol.* 21:268–278.

Lesh, M. D., J. F. Spear, and E. N. Moore. 1991. The importance of cell coupling and anisotropy to conduction in cardiac tissue. *In* Cardiac electrophysiology and arrhythmias. C. Fisch and B. Surawicz, editors. Elsevier, New York. 25–34.

Neunlist, M., and L. Tung. 1992. Evidence of oppositely polarized regions in the myocardium around a stimulating point electrode. *Circulation.* 84 Suppl II. II-667. (abstract).

Neunlist, M., and L. Tung. 1994a. Optical recordings of ventricular excitability of frog heart by an extracellular stimulating point electrode. *Pacing Clin. Electrophysiol.* 17:1641–1654.

Neunlist, M., and L. Tung. 1994b. Optical recordings of cardiac membrane potential around an extracellular electrode in electrically anisotropic, bullfrog atrium. *Proc. Ann. Int. Conf. IEEE Eng. Med. Biol. Soc.* 16: 43–44.

Neunlist, M., S.-Z. Zou, and L. Tung. 1992. Design and use of an optrode for optical recordings of cardiac action potentials. *Pfluegers Arch.* 420: 611–617.

Osaka, T., I. Kodama, N. Tsuboi, J. Toyama, and K. Yamada. 1987. Effects of activation sequence and anisotropic cellular geometry on the repolarization phase of action potential of dog ventricular muscles. *Circulation.* 76:226–236.

Plonsey, R., and R. C. Barr. 1988. Bioelectricity. Plenum Press, New York. 134.

Rattay, F. 1986. Analysis of models for external stimulation of axons. *IEEE Trans. Biomed. Eng.* 33:974–977.

Rattay, F. 1988. Modeling the excitation of fibers under surface electrodes. *IEEE Trans. Biomed. Eng.* 35:199–202.

Roberts, D. E., L. T. Hersh, and A. M. Scher. 1979. Influence of cardiac fiber orientation on wavefront voltage, conduction velocity, and tissue resistivity in the dog. *Circ. Res.* 44:701–712.

Roth, B. J. 1992. How the anisotropy of the intracellular and intracellular conductivities influences stimulation of cardiac muscle. *J. Math. Biol.* 30:633–646.

Roth, B. J., and N. Trayanova. 1993. Electrical stimulation in a time-dependent, passive bidomain. *Proc. Ann. Int. Conf. IEEE Eng. Med. Biol. Soc.* 15:857–858.

Roth, B. J., and J. P. Wikswo. 1994. Electrical stimulation of cardiac tissue: a bidomain model with active membrane properties. *IEEE Trans. Biomed. Eng.* 41:232–240.

Salama, G. 1988. Optical measurement of transmembrane potential in the heart. *In* Spectroscopic Membrane Probes, Vol. III. L. Loew, editor. CRC, Boca Raton, FL. 137–199.

Salama, G., and M. Morad. 1976. Merocyanine 540 as an optical probe of transmembrane potential activity in the heart. *Science.* 48:485–487.

Saypol, J. M., and B. J. Roth. 1992. A mechanism for anisotropic reentry in electrically active tissue. *J. Cardiovasc. Electrophysiol.* 3:558–566.

Sepulveda, N. G., B. J. Roth, and J. P. Wikswo. 1989. Current injection into a two-dimensional anisotropic bidomain. *Biophys. J.* 55:987–999.

Tanaka, I., and Y. Sasaki. 1966. On the electrotonic spread in cardiac muscle of the mouse. *J. Gen. Physiol.* 49:1089–1110.

Tung, L., M. Neunlist, and E. A. Sobie. 1994. Near-field and far-field stimulation of cardiac muscle. *In* Clinical Applications of Modern Imaging Technology II. L. J. Cerullo, K. S. Heiferman, H. Liu, H. Podbielska, A. O. Wist, L. J. Zamorano, and A. Katzir, eds. *Proc. Soc. Photo-Opt. Instrum. Eng.* 2132:367–374.

Tung, L., M. Neunlist, and S. Zou. 1991. Optical recordings of action potential of frog ventricle during cathodal and anodal stimulation. *Proc. Ann. Int. Conf. IEEE Eng. Med. Biol. Soc.* 13:603–604.

Walcott, G. P., K. T. Walcott, S. B. Knisley, X. Zhou, and R. E. Ideker. 1994. Mechanisms of defibrillation for monophasic and biphasic waveforms. *Pacing Clin. Electriophysiol.* 17:478–498.

Warman, E. N., W. M. Grill, and D. Durand. 1992. Modeling the effects of electric fields on nerve fibers: determination of excitation thresholds. *IEEE Trans. Biomed. Eng.* 39:1244–1254.

Wikswo, J. P., T. A. Wisialowski, W. A. Altmeier, J. R. Balser, H. A. Kopelman, and D. M. Roden. 1991. Virtual cathode effects during stimulation of cardiac muscle. *Circ. Res.* 68:513–530.

Wiley, J. D., and J. G. Webster. 1982. Analysis and control of the current distribution under circular dispersive electrodes. *IEEE Trans. Biomed. Eng.* 29:381–385.

Windisch, H., H. Ahammer, P. Shaffer, W. Müller, and D. Platzer. 1992. Fast optical potential mapping in single cardiomyocytes during field stimulation. *Proc. Ann. Int. Conf. IEEE Eng. Med. Biol. Soc.* 14:634–635.

Woodbury, J. W., and W. E. Crill. 1961. On the problem of impulse conduction in the atrium. *In Nervous Inhibition,* Lord Florey, ed. Plenum Press, New York. 124–135.